


Optimal Control of Short-Time Attractors in Active Nematics

Carlo Sinigaglia and Francesco Braghin 

Politecnico di Milano, Department of Mechanical Engineering, Milan 20156, Italy

Mattia Serra ^{*}

University of California San Diego, Department of Physics, San Diego, California 92093, USA

 (Received 28 April 2023; revised 17 April 2024; accepted 24 April 2024; published 22 May 2024)

Objective Eulerian coherent structures (OECs) and instantaneous Lyapunov exponents (iLEs) govern short-term material transport in fluid flows as Lagrangian coherent structures and the finite-time Lyapunov exponent do over longer times. Attracting OECs and iLEs reveal short-time attractors and are computable from the Eulerian rate-of-strain tensor. Here, we devise for the first time an optimal control strategy to create short-time attractors in compressible, viscosity-dominated active nematic flows. By modulating the active stress intensity, our framework achieves a target profile of the minimum eigenvalue of the rate-of-strain tensor, controlling the location and shape of short-time attractors. We show that our optimal control strategy effectively achieves desired short-time attractors while rejecting disturbances. Combining optimal control and coherent structures, our work offers a new perspective to steer material transport in compressible active nematics, with applications to morphogenesis and synthetic active matter.

DOI: [10.1103/PhysRevLett.132.218302](https://doi.org/10.1103/PhysRevLett.132.218302)

Large-scale coherent dynamics where global collective behaviors arise from local interactions, individual anisotropies, and activity are ubiquitous. Bird flocks, bacterial swarms or ensembles of cells exhibit macroscopic patterns whose length scale is orders of magnitude larger than the individual size [1–6]. The macroscopic dynamics of these systems of active individuals—or active matter—exhibit nonstandard physical properties such as self-organization, symmetry breaking, and nonreciprocity [2,7–10]. There are several descriptions of active matter [11], including agent-based models, coarse-grained continuum models, and data-driven models [12]. Besides studying the emergent properties of active matter, it is natural to ask how to control such systems.

The main possibilities rely on distributed or boundary control techniques [13]. Experimentally, Ross *et al.* [14] generated desired persistent fluid flows by regulating light patterns on a mixture of optogenetically modified motor proteins and microtubule filaments. Also controlling light, Lemma *et al.* [15] achieved spatiotemporal patterning of extensile active stresses in microtubule-based active fluids. By controlling an external electric field affecting cellular signaling networks, Cohen *et al.* [16] steered the collective motion of MDCK-II epithelial cells. From a theoretical perspective, Shankar *et al.* [17] propose a new framework to steer topological defects—the localized singularities in the orientation of the active building blocks [2]—by controlling activity stress patterns. Norton *et al.* [18] devised an optimal control problem (OCP) to achieve a target nematic director field by controlling either an applied vorticity field or the active stress magnitude in

incompressible active nematics. Alternative control strategies use surface anchoring at the boundaries and substrate drag to rectify the coherent flow of an active polar fluid in a 2D channel [19].

Existing theoretical methods target a desired configuration of the nematic director field, topological defects, or fluid velocities. While defects' dynamics drive large-scale chaotic flow [20–22], they may not be enough to predict spatiotemporal material transport. For instance, Serra *et al.* [23] show in experimental and numerical active nematics that the director field alone cannot predict if different domain regions will mix over a desired time interval or remain separated by a transport barrier, as well as predict where transport barriers are. In fact, even the knowledge of the velocity field and typical streamline or vorticity plots are suboptimal to studying material transport in unsteady flows, as shown in experimental and simulated velocities [24–26] and Fig. 1.

A natural framework to quantify material transport is the concept of coherent structures (CSs), see, e.g., [24,25,38], which serve as the robust frame-invariant skeletons shaping complex trajectory patterns. CSs such as attractors, their domain of attraction, and repellers are widespread in embryonic development across species [39–41] and active nematics [23]. Here, we devise for the first time an optimal control strategy to create short-time attractors in compressible, viscosity-dominated active nematic flows [40,42]. While most theory literature on active matter control assumes incompressible flows, in gastrulation and morphogenesis, flows are highly compressible, accounting for the internalization of cells to start organogenesis.

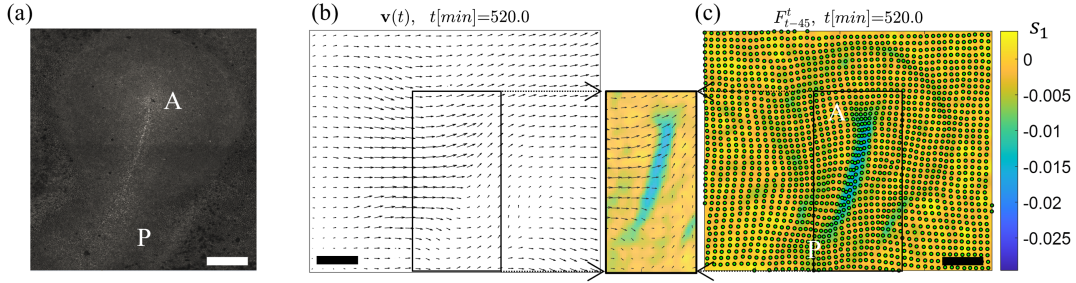


FIG. 1. Short-time attractors in an experimental multicellular flow. (a) Fluorescence image of the chicken embryo's epiblast, containing $\approx 60\,000$ cells during gastrulation. AP denotes the anterior-posterior axis. Velocities are reconstructed from light sheet microscopy [27]. The scale bar is $500\ \mu\text{m}$, and $t = 0$ corresponds to the beginning of gastrulation. (b) Velocity field $\mathbf{v}(\mathbf{x}, 520)$ (black vectors). (c) Instantaneous Lyapunov exponent field $s_1(\mathbf{x}, 520)$ (color map), consisting of the smallest eigenvalue of the rate-of-strain tensor of \mathbf{v} . Negative values of $s_1(\mathbf{x}, 520)$ mark short-time attractors. To visualize the effect of short-term attractors, green dots in panel (c) mark the current $t = 520$ position $\mathbf{F}_{475}^{520}(\mathbf{x}_0) = \mathbf{x}_0 + \int_{475}^{520} \mathbf{v}(\mathbf{F}_{475}^{\tau}, \tau) d\tau$ of short-time trajectories of $\mathbf{v}(\mathbf{x}, t)$, starting at $t = 475$ from a uniform spatial configuration. Within this short time ($45\ \text{min}/12\ \text{h} \approx 6\%$ of gastrulation time), trajectories accumulate on the $s_1(\mathbf{x}, 520)$ trench. The inset shows both $\mathbf{v}(\mathbf{x}, 520)$ and $s_1(\mathbf{x}, 520)$, highlighting how attractors remain hidden to \mathbf{v} but are correctly captured by s_1 . See Supplemental Material, Fig. S2 for the same analysis at a different time [28].

Material transport.—Long-term material transport is a Lagrangian phenomenon, originally studied by tracking the redistribution of individual trajectories. In that setting, the finite time Lyapunov exponent (FTLE) and Lagrangian coherent structures (LCSs) successfully predicted material transport [23,24,38,39,43,44]. An alternative to Lagrangian approaches is to find their instantaneous limits purely from Eulerian observations, avoiding the pitfalls of trajectory integration. Additionally, LCSs are impractical to control—no literature exists—because they are defined as nonlinear functions of fluid trajectories, which are integrals of the Eulerian velocity \mathbf{v} .

Short-time attractors—originally defined as attracting objective Eulerian coherent structures (OECSs) [25]—govern material transport in fluid flows over short times, revealing critical information in challenging problems such as search and rescue operations at sea [26] and oil-spill containment [45]. A simpler, more controllable alternative to attracting OECSs for locating short-time attractors is the instantaneous Lyapunov exponent (iLE) [46], defined as the instantaneous limit of the well-known FTLE. The iLE locates short-time attractors as trenches—or negative regions—of the smallest eigenvalue s_1 of the rate-of-strain tensor of the fluid velocity. For example, Fig. 1 shows short-term attractors marked by trenches of s_1 (scalar field) in an experimental velocity field (black vectors) describing the motion of thousands of cells during chick gastrulation [27]. A strong trench of s_1 marks a short-term attractor along the anterior-posterior (AP) axis corresponding to the forming primitive streak [39] [panel (c)], while remaining not identifiable from the inspection of the corresponding velocity field [panel (b) and inset]. Similar results hold in different flows (e.g., Fig. 1 of [25] and Figs. 4 and 5 of [26]).

This example shows that inspection and control of the velocity field \mathbf{v} is suboptimal to create material traps in

general unsteady flows. First, because the velocity field and its streamlines are not objective, i.e., they depend on the choice of reference frame used to describe motion (see also SM, Sec. 6 and Figs. S1–S2 [28]). By contrast, the location of material accumulation is frame invariant [24,25]. Second, it might be an unnecessarily strong requirement, or uncompliant with boundary conditions, to prescribe $\mathbf{v}(\mathbf{x}, t)$ directly.

Active fluid model.—We adopt a simplified version of the mechanochemical model developed in [40] consisting of an active Stokes flow characterized by the viscous stress $\boldsymbol{\sigma}_v = -p\mathbf{I} + 2\mu\mathbf{S}_d$ and active stress $\boldsymbol{\sigma}_a = m(\mathbf{B} - \mathbf{I}/2)$, where \mathbf{S}_d is the deviatoric rate-of-strain tensor, $\mathbf{B} = \mathbf{e} \otimes \mathbf{e}$ characterizes the orientation of active elements $\mathbf{e} = [\cos(\phi) \sin(\phi)]^T$, m denotes the intensity of active stress, and \mathbf{I} the identity tensor. To account for flow compressibility, we use a simple continuity equation $\nabla \cdot \mathbf{v} = c(-2p - p_0 m)$ where positive isotropic viscous stress ($p > 0$), and isotropic contractile-type ($m > 0$) active stress contribute to negative flow divergence via the bulk viscosity $1/c$ and a nondimensional parameter p_0 . Biologically, p_0 modulates the cell propensity to ingress into the third dimension given active isotropic apical contraction. The resulting system of PDEs in non-dimensional form [40] is

$$\begin{aligned} 2p_1 \Delta \mathbf{v} + \nabla[\nabla \cdot \mathbf{v}] + \mathbf{g}(m, \phi) &= \mathbf{0}, \\ \mathbf{g} &= p_1[2(\mathbf{B}\nabla m + m\nabla \cdot \mathbf{B}) + (p_0 - 1)\nabla m] = \nabla \cdot (\mathbf{A}m), \\ \phi_t &= -(\mathbf{v} \cdot \nabla)\phi + \frac{\omega}{2} + \left(\frac{u_y + v_x}{2} \cos 2\phi + \frac{v_y - u_x}{2} \sin 2\phi \right), \\ m_t &= -(\mathbf{v} \cdot \nabla)m + p_2(1 - me^{-\frac{p_3}{2}m}) + p_4 \Delta m, \end{aligned} \quad (1)$$

where $p_1 = \mu c$ is a second nondimensional parameter characterizing the ratio of the shear to bulk viscosity, $\mathbf{g}(m, \phi)$ is the active force, and $\mathbf{A} = 2p_1\mathbf{B} + p_1(p_0 - 1)\mathbf{I}$. The last two equations—not used here—model the dynamics

of the active stress intensity and orientation coupled to the tissue velocity in chick gastrulation [40,42].

Abstracting morphogenesis as a control problem, one can ask how embryos control their active stress to bring the right cells to specific spatiotemporal coordinates. This is precisely the case shown in Fig. 1, where mesoderm precursor cells converge to the attractors, marking the primitive streak [40]. As a first step, we consider a simplified dynamic where the orientation of active elements $\phi(\mathbf{x})$ is prescribed and time independent, and use the active stress intensity $m(\mathbf{x}, t)$ as the control input. A time-independent ϕ is a simplification that could be experimentally enforced by steady morphogen concentration inducing planar cell polarity or by imposing directional tension at the boundary [47]. How one might control m experimentally is system dependent. In microtubule-based active fluids, m can be controlled with light patterns [15]. By contrast, in the context of gastrulation—the most pertinent for our approach, given the viscous, compressible active nematic model [Eq. (1)]—we were able to indirectly control m *in vivo* in chick embryos by adding FGF2 (fibroblast growth factor 2) (see, e.g., Fig. 4 of [42], and SM S8 [28]). In *Drosophila*, m can be modulated by optogenetic activation or inhibition of Rho signaling [48–51].

Results.—To control short-time attractors, the OCP involves steering the minimum eigenvalue of the rate of strain tensor toward a target function while minimizing the overall control effort and its gradient:

$$\min_{m, \mathbf{v}} J_s = \frac{1}{2} \int_{\Omega} (s_1 - z)^2 d\Omega + \frac{\beta}{2} \int_{\Omega} (m^2 + \|\nabla m\|^2) d\Omega, \quad (2)$$

such that

$$\begin{aligned} -2p_1 \Delta \mathbf{v} - \nabla[\nabla \cdot \mathbf{v}] &= \mathbf{g}(m) + \mathbf{d} && \text{in } \Omega \\ \mathbf{v} &= \mathbf{0} && \text{on } \partial\Omega, \end{aligned}$$

where $z(\mathbf{x})$ represents a scalar target for the minimum eigenvalue $s_1(\mathbf{x})$ of the rate-of-strain tensor \mathbf{S} , $\mathbf{d}(\mathbf{x}, t)$ is an imposed known force (or disturbance), and Ω , $\partial\Omega$ denote the domain and its boundary, where we impose $\mathbf{v} = \mathbf{0}$. In

morphogenesis, \mathbf{d} could arise from external forces imposed on, rather than controlled by, the embryo. The optimal pair (\mathbf{v}, m) for the OCP (2) should satisfy the following system of first-order necessary conditions

$$\begin{aligned} -2p_1 \Delta \mathbf{v} - \nabla[\nabla \cdot \mathbf{v}] &= \mathbf{g}(m) + \mathbf{d} && \text{in } \Omega, \\ \mathbf{v} &= \mathbf{0} && \text{on } \partial\Omega, \\ -2p_1 \Delta \lambda - \nabla[\nabla \cdot \lambda] &= -\nabla \cdot ((s_1 - z)\xi_1 \otimes \xi_1) && \text{in } \Omega, \\ \lambda &= \mathbf{0} && \text{on } \partial\Omega, \\ -\beta \Delta m + \beta m - \nabla \lambda : \mathbf{A} &= 0 && \text{in } \Omega, \end{aligned} \quad (3)$$

where ξ_1 is the eigenvector field associated with s_1 (see SM, Secs. 2–4 for details [28]; SM includes Refs. [29–34], with additional information about the analysis and numerical solver of our OCP). Practically, at any t , given an imposed force distribution $\mathbf{d}(\mathbf{x}, t)$, boundary conditions and desired short-time attractor $z(\mathbf{x})$, (3) generates the optimal $m(\mathbf{x}, t)$ to achieve z . See SM, Sec. 8 for an algorithmic summary of (3) and a concrete application to avian-embryos morphogenesis [28]. Equation (3) requires an iterative method due to the complex nonlinear relationship between \mathbf{v} and the forcing term of the adjoint equation involving s_1 and ξ_1 . We solve (3) using a finite element method and a gradient-based algorithm (SM, Sec. 5 [28]) on a circular domain, and note that our algorithm applies to arbitrary domains.

We set the target shape z as a scaled indicator function of a rectangle so that the target value is -10 inside the rectangle and zero elsewhere. We set the cable orientation to a constant value $\phi = (\pi/4)$ from the x axis and choose the control weighting parameter $\beta = 10^{-6}$ and the non-dimensional model parameters $p_0 = 10$, $p_1 = 0.5$. p_1 modulates the overall fluid compressibility while high p_0 induces high negative divergence in regions with higher m [40]. We select the space-time varying disturbance force as $\mathbf{d}(\mathbf{x}, t) = d e^{-(r(t)/\sigma)^2} \{-[y - y_c(t)], x - x_c(t)\}$, where $\mathbf{x}_c(t) = [-0.5 + t, 0.5]$, $r(t) = \|\mathbf{x} - \mathbf{x}_c(t)\|$, and set the intensity $d = 50$, and standard deviation $\sigma = 0.2$.

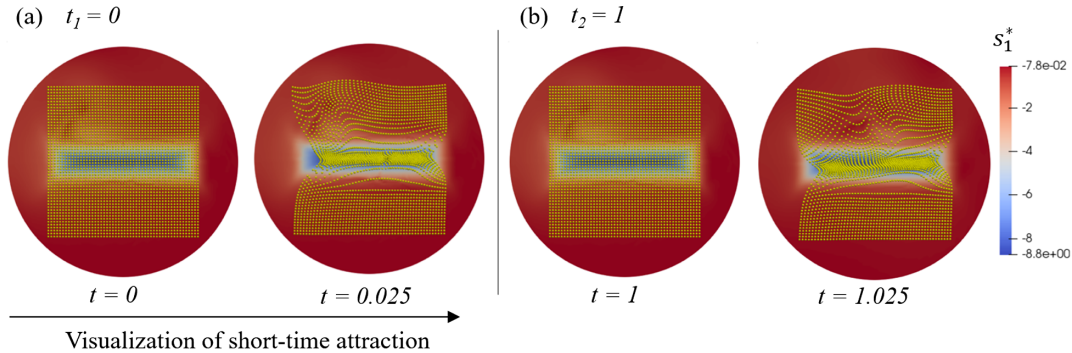


FIG. 2. Optimal solution of the OCP generating short-time attractors. The target minimum eigenvalue $z(\mathbf{x})$ is the indicator function of a rectangle at the center of the domain. The optimal eigenvalue field $s_1^*(\mathbf{x})$ is shown by the color map. (a),(b) correspond to different initialization times t_i and show the effect of short-time attractors by initializing a uniform set of fluid tracers (yellow dots) at each t_i and displaying their later positions integrating $\mathbf{v}(\mathbf{x}, t)$ over short times, as in Figs. 1(c).

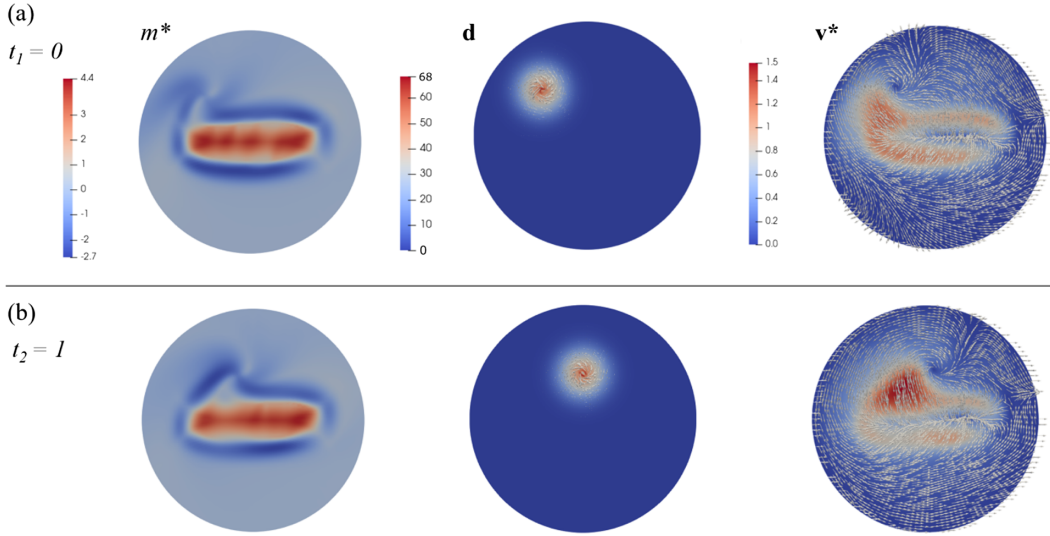


FIG. 3. Optimal control state pair (m^* , \mathbf{v}^*) and moving imposed (or disturbance) \mathbf{d} associated to the OCP described in Fig. 2. \mathbf{d} and \mathbf{v}^* are vector fields (arrows) with their magnitude also displayed in the color map. The \mathbf{v}^* vectors are normalized to ease visualization. Each row (a),(b) corresponds to different initialization times t_i as Fig. 2. The velocity dynamics \mathbf{v} are strongly affected by the presence of the disturbance.

Figure 2 shows the resulting optimal s_1 along with a grid of particles advected over short times for two different initialization times. Figure 3 shows the optimal state-control pair and its associated disturbance \mathbf{d} . The control m acts through $\mathbf{g}(m) = \nabla \cdot (\mathbf{A}m)$, and therefore both m and ∇m contribute to the state dynamics. Overall, the disturbance strongly influences the optimal velocity.

Figure 4 shows the interplay between the control weight β , the disturbance \mathbf{d} , and the accuracy of the tracking objective. To present an additional test case, we select a

different disturbance compared to Figs. 2 and 3, generating two vortex-shaped force-field streamlines (Fig. 4, first column) using the same functional form in the previous test case. The target eigenvalue z is the same as in Figs. 2 and 3. The uncontrolled dynamics ($m = 0$) does not generate attraction (Fig. 4, second column), while weak and strong control (third-fourth columns) steer s_1 toward the target, generating a material trap while rejecting \mathbf{d} . In SM, S7 [28], we provide an extensive sensitivity analysis and show that our control scheme can generate any attractor geometry

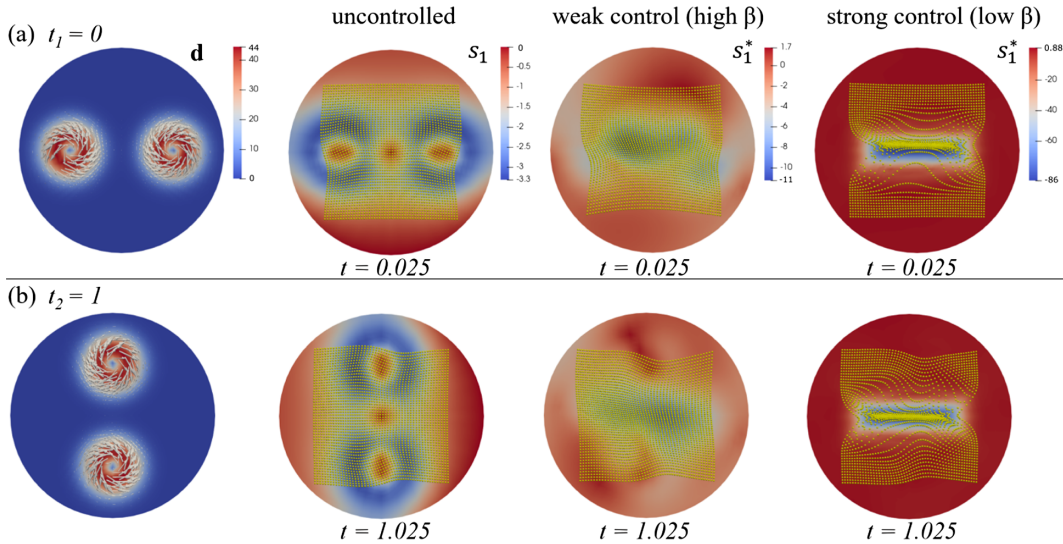


FIG. 4. Controlled and uncontrolled dynamics for two spatiotemporal disturbances $\mathbf{d}(\mathbf{x}, t_i)$ (first column). Columns 2–4 show $s_1(\mathbf{x})$ for no control, weak ($\beta = 0.1$), and strong ($\beta = 10^{-6}$) control along with fluid tracers advected for a short time starting from a uniform initial grid at t_i . Here, $\mathbf{d}(\mathbf{x}, t) = \mathbf{d}[\mathbf{x}_{c1}(t)] - \mathbf{d}[\mathbf{x}_{c2}(t)]$, where $\mathbf{x}_{c1}(t) = 0.5[\cos(0.5\pi t) + \pi, \cos(0.5\pi t) + \pi]$, $\mathbf{x}_{c2}(t) = 0.5[\cos(0.5\pi t), \cos(0.5\pi t)]$, and $\mathbf{d}[\mathbf{x}_{ci}(t)] = \{-[y - y_{ci}(t)], [x - x_{ci}(t)]\}500 \exp\{-[(x - x_{ci}(t))^2 + (y - y_{ci}(t))^2]/0.2^2\}$.

and is robust to changes in control and model parameters, the orientation of active elements ϕ , and the disturbance \mathbf{d} . In SM, S8, we illustrate our approach in the context of avian gastrulation control, where \mathbf{d} represents a traction force imposed on the embryo by extraembryonic cells, and the embryo develops a ring-shaped, short-time attractor by modulating its active myosin distribution m , consistent with *in vivo* experiments in the chick embryo [40,42] (see Supplemental Material [28], which includes Refs. [35–37], for additional information on chick gastrulation).

Conclusion.—We have proposed an optimal control problem that generates, for the first time, material short-time attractors at desired locations in compressible, highly viscous active nematics using the active stress intensity as the control input. Short-time attractors predict the correct location of material attraction, which may be undetected from the inspection of frame-dependent velocity fields (Fig. 1, [25,26]). Additionally, several configurations of the frame-dependent \mathbf{v} can generate the same frame-invariant attractor configurations (see, e.g., Figs. S3–S5 [28]). Similarly, one can control material repellers, which, together with attractors, shape complex motion in synthetic active matter [23] and living embryos [39,41]. Our results demonstrate how to achieve these aims in principal. As experimental techniques to manipulate m increase in their precision and availability in more systems, this theoretical technique may enable the creation of material traps for medical applications as well as enhance our ability to control morphogenetic flows. For example, it will shed light on how myosin activity (active stress intensity) generates the required motion that compartmentalizes the embryo, segregating distinct cell types (repellers) and steering specific cells to precise locations (attractors). In future work, we plan to consider the explicit orientational dynamics of the active stress anisotropy, the effect of inertial forces, and the control of Lagrangian coherent structures that shape fluid motion over longer times.

We acknowledge Manli Chuai, Guillermo Serrano Nájera, and Kees Weijer for the experimental data in Fig. 1 and SM S8, and Alex Plum for his comments on the manuscript. M. S. acknowledges financial support from the Hellman Foundation.

*mserra@ucsd.edu

- [1] J. Toner and Y. Tu, Long-range order in a two-dimensional dynamical XY model: How birds fly together, *Phys. Rev. Lett.* **75**, 4326 (1995).
- [2] M. C. Marchetti, J. F. Joanny, S. Ramaswamy, T. B. Liverpool, J. Prost, M. Rao, and R. A. Simha, Hydrodynamics of soft active matter, *Rev. Mod. Phys.* **85**, 1143 (2013).
- [3] K. Kruse, J. F. Joanny, F. Jülicher, J. Prost, and K. Sekimoto, Asters, vortices, and rotating spirals in active gels of polar filaments, *Phys. Rev. Lett.* **92**, 078101 (2004).
- [4] M. Ballerini, N. Cabibbo, R. Candelier, A. Cavagna, E. Cisbani, I. Giardina, V. Lecomte, A. Orlandi, G. Parisi, A. Procaccini *et al.*, Interaction ruling animal collective behavior depends on topological rather than metric distance: Evidence from a field study, *Proc. Natl. Acad. Sci. U.S.A.* **105**, 1232 (2008).
- [5] A. Bricard, J. Caussin, N. Desreumaux, O. Dauchot, and D. Bartolo, Emergence of macroscopic directed motion in populations of motile colloids, *Nature (London)* **503**, 95 (2013).
- [6] C. Dombrowski, L. Cisneros, S. Chatkaew, R. E. Goldstein, and J. O. Kessler, Self-concentration and large-scale coherence in bacterial dynamics, *Phys. Rev. Lett.* **93**, 098103 (2004).
- [7] S. Ramaswamy, Active matter, *J. Stat. Mech.* (2017) 054002.
- [8] M. Fruchart, R. Hanai, P. B. Littlewood, and V. Vitelli, Non-reciprocal phase transitions, *Nature (London)* **592**, 363 (2021).
- [9] M. J. Bowick, N. Fakhri, M. C. Marchetti, and S. Ramaswamy, Symmetry, thermodynamics, and topology in active matter, *Phys. Rev. X* **12**, 010501 (2022).
- [10] S. Shankar, A. Souslov, M. J. Bowick, M. C. Marchetti, and V. Vitelli, Topological active matter, *Nat. Rev. Phys.* **4**, 380 (2022).
- [11] M. R. Shaebani, A. Wysocki, R. G. Winkler, G. Gompper, and H. Rieger, Computational models for active matter, *Nat. Rev. Phys.* **2**, 181 (2020).
- [12] C. Joshi, S. Ray, L. M. Lemma, M. Varghese, G. Sharp, Z. Dogic, A. Baskaran, and M. F. Hagan, Data-driven discovery of active nematic hydrodynamics, *Phys. Rev. Lett.* **129**, 258001 (2022).
- [13] A. Manzoni, S. Salsa, and A. Quarteroni, *Optimal Control of Partial Differential Equations, Analysis, Analysis, Approximation and Applications* (Springer, New York, 2021).
- [14] T. D. Ross, H. J. Lee, Z. Qu, R. A. Banks, R. Phillips, and M. Thomson, Controlling organization and forces in active matter through optically defined boundaries, *Nature (London)* **572**, 224 (2019).
- [15] L. M. Lemma, M. Varghese, T. D. Ross, M. Thomson, A. Baskaran, and Z. Dogic, Spatio-temporal patterning of extensible active stresses in microtubule-based active fluids, *PNAS Nexus* **2**, pgad130 (2023).
- [16] D. J. Cohen, W. James Nelson, and M. M. Maharbiz, Galvanotactic control of collective cell migration in epithelial monolayers, *Nat. Mater.* **13**, 409 (2014).
- [17] S. Shankar, L. V. Scharrer, M. J. Bowick, and M. C. Marchetti, Spatiotemporal control of active topological defects, *arXiv:2212.00666*.
- [18] M. M. Norton, P. Grover, M. F. Hagan, and S. Fraden, Optimal control of active nematics, *Phys. Rev. Lett.* **125**, 178005 (2020).
- [19] P. Gulati, S. Shankar, and M. C. Marchetti, Boundaries control active channel flows, *Front. Phys.* **10**, 948415 (2022).
- [20] L. Giomi, Geometry and topology of turbulence in active nematics, *Phys. Rev. X* **5**, 031003 (2015).
- [21] S. Shankar and M. C. Marchetti, Hydrodynamics of active defects: From order to chaos to defect ordering, *Phys. Rev. X* **9**, 041047 (2019).

- [22] A. J. Tan, E. Roberts, S. A. Smith, U. A. Olvera, J. Arteaga, S. Fortini, K. A. Mitchell, and L. S. Hirst, Topological chaos in active nematics, *Nat. Phys.* **15**, 1033 (2019).
- [23] M. Serra, L. Lemma, L. Giomi, Z. Dogic, and L. Mahadevan, Defect-mediated dynamics of coherent structures in active nematics, *Nat. Phys.* **19**, 1355 (2023).
- [24] G. Haller, Lagrangian coherent structures, *Annu. Rev. Fluid Mech.* **47**, 137 (2015).
- [25] M. Serra and G. Haller, Objective eulerian coherent structures, *Chaos* **26**, 053110 (2016).
- [26] M. Serra, P. Sathe, I. Rypina, A. Kirincich, S. D. Ross, P. Lermusiaux, A. Allen, T. Peacock, and G. Haller, Search and rescue at sea aided by hidden flow structures, *Nat. Commun.* **11**, 1 (2020).
- [27] E. Rozbicki, M. Chuai, A. Karjalainen, F. Song, H. Sang, R. Martin, H. Knölker, M. MacDonald, and C. Weijer, Myosin-II-mediated cell shape changes and cell intercalation contribute to primitive streak formation, *Nat. Cell Biol.* **17**, 397 (2015).
- [28] See Supplemental Material at <http://link.aps.org/supplemental/10.1103/PhysRevLett.132.218302>, which includes Refs. [29–34], for additional information about the analysis and numerical solver of our OCP, and which also includes Refs. [35–37], for additional information on chick gastrulation.
- [29] S. Salsa, *Partial Differential Equations in Action: From Modelling to Theory* (Springer, New York, 2016), Vol. 99.
- [30] R. A. Horn and C. R. Johnson, *Matrix Analysis* (Cambridge University Press, Cambridge, England, 2012).
- [31] D. Arndt, W. Bangerth, B. Blais, M. Fehling, R. Gassmüller, T. Heister, L. Heltai, U. Köcher, M. Kronbichler, M. Maier, P. Munch, J.-P. Pelteret, S. Proell, K. Simon, B. Turcksin, D. Wells, and J. Zhang, The deal.II library, version 9.3, *J. Numer. Math.* **29**, 171 (2021).
- [32] S. G. Johnson, The NLOpt Nonlinear-Optimization Package (2011), <http://ab-initio.mit.edu/nlopt>.
- [33] M. Gurtin, *An Introduction to Continuum Mechanics* (Academic Press, New York, 1982), Vol. 158.
- [34] B. Chachuat, Nonlinear and dynamic optimization: From theory to practice, Technical Report, 2007.
- [35] D. New, The adhesive properties and expansion of the chick blastoderm, *Development* **7**, 146 (1959).
- [36] H. C. Lee, Y. Fadaili, and C. D. Stern, Molecular characteristics of the edge cells responsible for expansion of the chick embryo on the vitelline membrane, *Open Biol.* **12**, 220147 (2022).
- [37] J. Downie, The mechanism of chick blastoderm expansion, *Development* **35**, 559 (1976).
- [38] A. Hadjighasem, M. Farazmand, D. Blazeovski, G. Froyland, and G. Haller, A critical comparison of Lagrangian methods for coherent structure detection, *Chaos* **27**, 053104 (2017).
- [39] M. Serra, S. Streichan, M. Chuai, C. J. Weijer, and L. Mahadevan, Dynamic morphoskeletons in development, *Proc. Natl. Acad. Sci. U.S.A.* **117**, 11444 (2020).
- [40] M. Serra, G. Serrano Nájera, M. Chuai, A. M. Plum, S. Santhosh, V. Spandan, C. J. Weijer, and L. Mahadevan, A mechanochemical model recapitulates distinct vertebrate gastrulation modes, *Sci. Adv.* **9**, eadh8152 (2023).
- [41] M. Lange, A. Granados, S. VijayKumar, J. Bragantini, S. Ancheta, S. Santhosh, M. Borja, H. Kobayashi, E. McGeever, A. C. Solak *et al.*, Zebrahub-multimodal zebrafish developmental atlas reveals the state transition dynamics of late vertebrate pluripotent axial progenitors, *bioRxiv* (2023).
- [42] M. Chuai, G. Serrano Nájera, M. Serra, L. Mahadevan, and C. J. Weijer, Reconstruction of distinct vertebrate gastrulation modes via modulation of key cell behaviors in the chick embryo, *Sci. Adv.* **9**, eabn5429 (2023).
- [43] S. Shadden, F. Lekien, and J. E. Marsden, Definition and properties of Lagrangian coherent structures from finite-time Lyapunov exponents in two-dimensional aperiodic flows, *Physica (Amsterdam)* **212D**, 271 (2005).
- [44] M. Serra, P. Sathe, F. Beron-Vera, and G. Haller, Uncovering the edge of the polar vortex, *J. Atmos. Sci.* **74**, 3871 (2017).
- [45] R. Duran, T. Nordam, M. Serra, and C. H. Barker, Horizontal transport in oil-spill modeling, in *Marine Hydrocarbon Spill Assessments* (Elsevier, New York, 2021), pp. 59–96.
- [46] P. J. Nolan, M. Serra, and S. D. Ross, Finite-time Lyapunov exponents in the instantaneous limit and material transport, *Nonlinear Dyn.* **100**, 3825 (2020).
- [47] D. Kunz, A. Wang, C. U. Chan, R. H. Pritchard, W. Wang, F. Gallo, C. R. Bradshaw, E. Terenzani, K. H. Müller, Y. Y. S. Huang *et al.*, Downregulation of extraembryonic tension controls body axis formation in avian embryos, *Nat. Commun.* **14**, 3266 (2023).
- [48] G. Guglielmi, J. D. Barry, W. Huber, and S. De Renzis, An optogenetic method to modulate cell contractility during tissue morphogenesis, *Dev. Cell* **35**, 646 (2015).
- [49] E. Izquierdo, T. Quinkler, and S. De Renzis, Guided morphogenesis through optogenetic activation of Rho signalling during early drosophila embryogenesis, *Nat. Commun.* **9**, 2366 (2018).
- [50] H. J. Gustafson, N. Claussen, S. De Renzis, and S. J. Streichan, Patterned mechanical feedback establishes a global myosin gradient, *Nat. Commun.* **13**, 7050 (2022).
- [51] H. Guo, M. Swan, and B. He, Optogenetic inhibition of actomyosin reveals mechanical bistability of the mesoderm epithelium during drosophila mesoderm invagination, *eLife* **11**, e69082 (2022).